Electrochimica Acta 484 (2024) 143957

Contents lists available at ScienceDirect

Electrochimica Acta

journal homepage: www.journals.elsevier.com/electrochimica-acta

Redox mediated enhancement and quenching of co-reactant electrochemiluminescence by iridium(III) complexes

Steven J. Blom [a,1], Natasha S. Adamson [a,1], Emily Kerr [b], Egan H. Doeven [a], Oliver S. Wenger [c], Raoul S. Schaer [c], David J. Hayne [b], Francesco Paolucci [d], Neso Sojic [e], Giovanni Valenti [d], Paul S. Francis [a,*]

[a] Centre for Sustainable Bioproducts, Faculty of Science, Engineering and Built Environment, Deakin University, Geelong, Victoria 3220, Australia
[b] Institute for Frontier Materials, Deakin University, Geelong, Victoria 3220, Australia
[c] Department of Chemistry, University of Basel, St. Johanns-Ring 19, 4056 Basel, Switzerland
[d] Department of Chemistry Giacomo Ciamician, University of Bologna, via Selmi 2, Bologna 40126, Italy
[e] Univ. Bordeaux, CNRS, Bordeaux INP, Institut des Sciences Moléculaires, UMR 5255, 33607 Pessac, France

ARTICLE INFO

Keywords:
Electrochemiluminescence
Electrogenerated chemiluminescence
Redox mediator
Water-soluble iridium(III) complex

ABSTRACT

Enhancement of the electrochemiluminescence (ECL) of tris(2,2′-bipyridine)ruthenium(II) ($[Ru(bpy)_3]^{2+}$) and tri-*n*-propylamine by redox mediators has emerged as a new approach to maximise the sensitivity of this mode of detection. Herein, we examine the influence of six water-soluble iridium(III) complexes on this widely used ECL system by deconvoluting their respective contributions to the overall ECL intensity over a range of applied potentials. The interconnected co-reactant ECL of these metal complexes, eliciting enhancement or quenching of the $[Ru(bpy)_3]^{2+}$ emission, can be understood by considering the available reaction pathways under different conditions and the disparate electrochemical and photophysical properties of the reactants. The ideal properties for enhancement are established, which will inform the future design and application of redox mediators in this ECL system.

1. Introduction

Electrochemiluminescence (ECL) is a highly sensitive mode of detection, in which electrochemically generated reactants form electronically excited species that emit light to return to the ground state [1]. Most ECL applications and commercially available ECL assay systems make use of the tris(2,2′-bipyridine)ruthenium(II) ($[Ru(bpy)_3]^{2+}$) and tri-*n*-propylamine (TPrA) 'co-reactant' mechanism that is outlined in Schemes 1–4 (Fig. 1, where M = $[Ru(bpy)_3]^{2+}$) [2–7]. Upon application of a suitable electrochemical potential to oxidise both reactants, the emitting species can be generated by reaction between the oxidised metal complex and the α-amino alkyl radical ($TPrA^{\bullet}$) derived by deprotonation after the oxidation of TPrA (Scheme 1, where M = $[Ru(bpy)_3]^{2+}$). Oxidation of the co-reactant may be heterogeneous (Schemes 1, 3–5) or homogeneous (Scheme 2). $TPrA^{\bullet}$ can also reduce $[Ru(bpy)_3]^{2+}$, enabling the 'annihilation' ECL reaction between $[Ru(bpy)_3]^{+}$ and electrogenerated $[Ru(bpy)_3]^{3+}$ (Scheme 3). The pathways shown in Schemes 2 and 3, however, make only minor contributions to the ECL intensity when $[Ru(bpy)_3]^{2+}$ is at relatively low concentrations [8].

At potentials at which only the co-reactant is oxidised, ECL can still be observed because the aminium radical cation, $TPrA^{\bullet+}$, is a sufficiently strong oxidant to generate the excited state luminophore from $[Ru(bpy)_3]^{+}$ (Scheme 4) [5]. This pathway is critical for ECL detection in the widely used bead-supported assay format [11–13], where the vast majority of the metal complexes are bound at distances from the electrode that do not permit their direct oxidation, irrespective of the applied potential.

Attempts to enhance this detection system have included the development of new co-reactants, which exhibit advantages under certain circumstances [12,14-18]. To date, however, none of these have been found to be superior to TPrA for bead-based assays. The ECL signal of the $[Ru(bpy)_3]^{2+}$ luminophore has been amplified using dendrimer or nanoparticle labels with multiple metal-complex centres [19–22], but their relative complexity, non-linear improvement in intensity and/or

* Corresponding author.
E-mail address: paul.francis@deakin.edu.au (P.S. Francis).
[1] These authors contributed equally.

https://doi.org/10.1016/j.electacta.2024.143957
Received 18 December 2023; Received in revised form 21 January 2024; Accepted 13 February 2024
Available online 14 February 2024

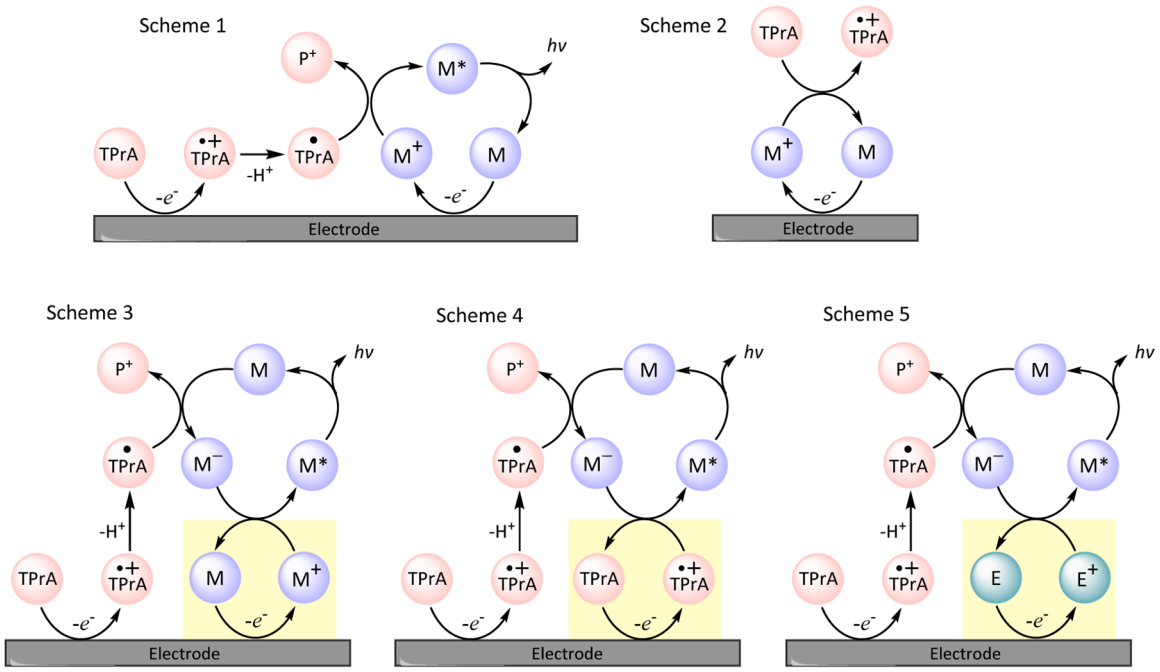

Fig. 1. Reaction pathways for certain transition metal complexes (M and E) with tri-*n*-propylamine (TPrA; E_{ox} = 0.89 V vs Ag/AgCl) [5] as a co-reactant, where $TPrA^{\bullet+}$ is $Pr_3N^{\bullet+}$, $TPrA^{\bullet}$ is $Pr_2NC^{\bullet}HCH_2CH_3$, and P^+ is $Pr_2N^+{=}CHCH_2$, an iminium cation that hydrolyses in aqueous solution [5,6,9,10]. ***Scheme 1***: The 'direct' route, requiring electrooxidation of the metal complex. ***Scheme 2***: The 'catalytic' route, in which TPrA is homogeneously oxidised. ***Scheme 3***: Reaction of the electrochemically oxidised and chemically reduced luminophore, analogous to 'annihilation ECL' in which both species are electrogenerated. ***Scheme 4***: The 'indirect' route (or 'remote' or 'low-oxidation potential' pathway), in which TPrA is oxidised at the electrode. ***Scheme 5***: The 'redox-mediator' route [9,10], in which an additional electrooxidised species (E^+) can react with the reduced luminophore to generate the emissive species. As highlighted by the yellow boxes, an analogous role is played by the luminophore or co-reactant in established ECL pathways, but the new metal complex (E) can be added at higher concentrations and oxidised at lower potentials than M, and form a more stable oxidised species (E^+) than $TPrA^{\bullet+}$. The redox-mediator may also serve as alternative to the luminophore in the homogeneous oxidation of $TPrA^{\bullet+}$ in Scheme 2.

higher background responses due to nonspecific binding has limited application of this approach. Numerous Ir(III) complexes have been explored as ECL active luminophores, offering high quantum yields and a wide range of emission colours [23–25]. In many cases, however, their redox potentials do not permit ECL without electrochemical oxidation of the metal complex (i.e. Scheme 4 is not thermodynamically feasible; where M = Ir(III) complex) [26], and very few of those reported are soluble in aqueous solution.

Strategies to impart water-solubility to Ir(III) complexes for ECL and other applications most commonly involve decoration of the coordinating ligands with hydrophilic functional groups such as sulfonates and tetraethylene glycol [27–31]. Various $[Ir(C\hat{}N)_2(pt\text{-}TEG)]^+$ complexes (Fig. 2a), for example, elicit similar ECL intensities to $[Ru(bpy)_3]^{2+}$ with TPrA in aqueous solution at high applied potentials, and have been adapted for ECL labelling [29].

Recently we reported that despite its poor co-reactant ECL intensity, the *fac*-$[Ir(sppy)_3]^{3-}$ complex (Fig. 2b) could enhance the co-reactant ECL of $[Ru(bpy)_3]^{2+}$ by over an order of magnitude at potentials where only the Ir(III) complex and TPrA were oxidised [9]. This was ascribed to a 'redox mediator' pathway (analogous to Schemes 3 and 4), in which reaction between $[Ru(bpy)_3]^+$ and the electrogenerated $[Ir(sppy)_3]^{2-}$ is sufficiently energetic to generate the excited state $[Ru(bpy)_3]^{2+*}$ species (Scheme 5, where M = $[Ru(bpy)_3]^{2+}$ and E = $[Ir(sppy)_3]^{3-}$). Importantly, like Scheme 4, this pathway does not require electro-oxidation of $[Ru(bpy)_3]^{2+}$ and, therefore, effective translation to bead-based ECL assays was anticipated [9]. Indeed, $[Ir(sppy)_3]^{3-}$ was shown to enhance the ECL of $[Ru(bpy)_3]^{2+}$ immobilised on 12 μm polystyrene beads by over 70-fold at 0.9 V vs Ag/AgCl, and 2.9-fold at 1.2 V vs Ag/AgCl [10]. The larger effect under these conditions likely arises from the greater dependence on the lifetime of the $TPrA^{\bullet+}$, which must diffuse from the electrode surface to reduce the immobilised luminophore (Scheme 4).

Moreover, as the $[Ru(bpy)_3]^{2+}$ labels are too distant from the working electrode to be oxidised, the lower enhancement by $[Ir(sppy)_3]^{3-}$ at 1.2 V vs Ag/AgCl cannot be rationalised by the dominance of Scheme 1 at high potentials. Instead, this indicates a significant contribution from the catalytic oxidation of TPrA (Scheme 2, where M = $[Ir(sppy)_3]^{3-}$) at low potentials, which diminishes in importance at high potentials with the increased rate of its direct electrochemical oxidation [10,32].

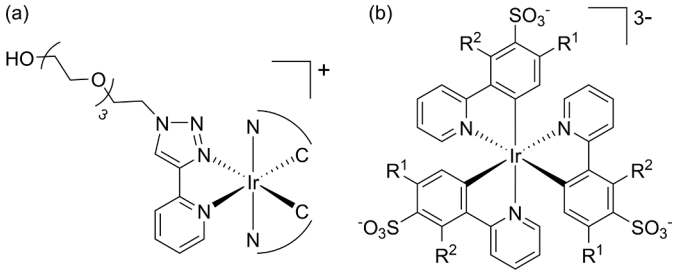

C^N	Complex
bt	$[Ir(bt)_2(pt\text{-}TEG)]^+$
ppy	$[Ir(ppy)_2(pt\text{-}TEG)]^+$
df-ppy	$[Ir(df\text{-}ppy)_2(pt\text{-}TEG)]^+$

R^1	R^2	Complex
H	H	$[Ir(sppy)_3]^{3-}$
F	H	$[Ir(f\text{-}sppy)_3]^{3-}$
F	F	$[Ir(df\text{-}sppy)_3]^{3-}$

Fig. 2. Structures of water-soluble Ir(III) complexes examined in this study (bt = 2-(2-benzothiazolyl-κ*N*^{3})phenyl-κ*C*; ppy = 2-(2-pyridinyl-κ*N*)phenyl-κ*C*; df-ppy = 3,5-difluoro-2-(2-pyridinyl-κ*N*)phenyl-κ*C*; pt-TEG = 3-(2-(2-(2-(2-hydroxyethoxy)ethoxy)ethoxy)ethyl)−5-(2-pyridinyl-κ*N*)−1*H*-1,2,3λ^4-triazol-1-yl-κ*N*; sppy = 2-(2-pyridinyl-κ*N*)−4-sulfonatophenyl-κ*C*; f-sppy = 5-fluoro-2-(2-pyridinyl-κ*N*)−4-sulfonatophenyl-κ*C*; df-sppy = 3,5-difluoro-2-(2-pyridinyl-κ*N*)−4-sulfonatophenyl-κ*C*).

Subsequent ECL microscopy of $[Ru(bpy)_3]^{2+}$ immobilised on 2.8 μm magnetic beads upon application of 1.2 V vs Ag/AgCl showed a 2-fold enhancement by 100 μM $[Ir(sppy)_3]^{3-}$, but considerable quenching by the same concentration of $[Ir(bt)_2(pt\text{-}TEG)]^+$ or $[Ir(df\text{-}ppy)_2(pt\text{-}TEG)]^+$ (Fig. 2a) [32]. The contrasting behaviour of these complexes was rationalised by the differences in their redox potentials where, unlike $[Ir(sppy)_3]^{3-}$, these two $[Ir(C^N)_2(pt\text{-}TEG)]^+$ complexes may react with $TPrA^\bullet$ (consuming this key intermediate of Scheme 4). Furthermore, both of these complexes are oxidised at potentials greater than that of $[Ru(bpy)_3]^{2+}$, and therefore Scheme 5 (where M = $[Ru(bpy)_3]^{2+}$ and E = the Ir(III) complex) cannot occur at low potentials.

Herein we examine the influence of these Ir(III) complexes under homogeneous reaction conditions, which removes the mechanistic constraints of $[Ru(bpy)_3]^{2+}$ luminophore immobilisation. In addition, we explore alternative Ir(III) species $[Ir(ppy)_2(pt\text{-}TEG)]^+$, $[Ir(f\text{-}sppy)_3]^{3-}$ and $[Ir(df\text{-}sppy)_3]^{3-}$ (Fig. 2), which like $[Ir(sppy)_3]^{3-}$, are oxidised at potentials lower than that of $[Ru(bpy)_3]^{2+}$, and reduced at potentials beyond that estimated for the oxidation of $TPrA^\bullet$. These investigations provide a new understanding of the action of Ir(III) redox mediators in the classic and most widely used $[Ru(bpy)_3]^{2+}$-TPrA co-reactant ECL system.

2. Experimental

2.1. Chemicals

All reagents and solvents were purchased from commercial sources and used without further purification. Bis(cyclopentadienyl)iron (ferrocene, 99%) and tris(2,2′-bipyridine)ruthenium(II) dichloride hexahydrate ($[Ru(bpy)_3]Cl_2{\cdot}6H_2O$) were from Strem (USA). The sodium salt of *fac*-$[Ir(sppy)_3]^{3-}$ was from Lumtec (Taiwan). $Na_3[Ir(f\text{-}sppy)_3]$, $Na_3[Ir(df\text{-}sppy)_3]$, $[Ir(bt)_2(pt\text{-}TEG)]Cl$, $[Ir(ppy)_2(pt\text{-}TEG)]Cl$, and $[Ir(df\text{-}ppy)_2(pt\text{-}TEG)]Cl$ were synthesised as previously reported [29,33]. Tri-*n*-propylamine (TPrA), potassium phosphate monobasic, potassium phosphate dibasic, and tetrabutylammonium hexafluorophosphate ($TBAPF_6$, 99% electrochemical grade), were sourced from Sigma-Aldrich (Australia). ProCell buffer solution was purchased from Roche Australia.

2.2. Spectroscopy

Absorption spectra were acquired using a Cary 300 Bio UV/Vis spectrophotometer (600 nm min^{-1}, 2 nm bandwidth; Agilent, Australia). Photoluminescence (PL) spectra were measured using a Cary Eclipse fluorescence spectrophotometer (600 nm min^{-1}, 5 nm bandwidth; Agilent). Each measurement was obtained in a quartz cuvette with 1 cm path length using 10 μM complex in ultrapure (milli-Q) water. Low-temperature (85 K) PL spectra were obtained using the Eclipse spectrophotometer with an OptistatDN Variable Temperature Liquid Nitrogen Cryostat (Oxford Instruments, UK) equipped with a custom-made quartz sample holder [34]. The metal complexes were prepared at 5 μM in 4:1 ethanol:methanol and cooled to 85 K. Further cooling was not undertaken to avoid damage to the cuvettes due to the change in solvent volume as it approaches 77 K [35]. We previously found no change in the wavelengths of maximum emission for $[Ru(bpy)_3]^{2+}$ and $Ir(ppy)_3$ between these two temperatures [34]. Correction factors for the PL spectra established using a quartz halogen tungsten lamp were used to account for variation in instrumental sensitivity over the wavelength range.

2.3. Electrochemistry

Electrochemical experiments were performed using a cylindrical cell [36] equipped with glassy carbon working, platinum wire counter (CH Instruments), and leakless Ag/AgCl reference (model ET069; eDAQ Australia) electrodes. Prior to each measurement, the working electrode was polished using 0.05 μm alumina powder (CH Instruments) and rinsed with ethanol and water; the counter electrode was flamed using a blowtorch; and the reference electrode was rinsed with water. Measurements were performed using an Autolab PGSTAT204 or Autolab PGSTAT128N (CH Instruments), and data was recorded using Nova software (version 1.11). Cyclic voltammograms were collected at a scan rate of 0.1 V/s in either DMF with 0.1 M $TBAPF_6$ as supporting electrolyte, or 0.1 M phosphate buffer solution (PBS; pH 7.5).

2.4. Electrochemiluminescence

Experiments were performed in ProCell solution (containing 180 mM TPrA co-reactant, 0.1% surfactant and a preservative in 0.3 M phosphate buffer at pH 6.8) [37]. The emitted light was measured by interfacing the electrochemical cell with either: a photomultiplier tube (PMT, extended-range trialkali S20, ET Enterprises model 9828B) for intensity; a charge coupled device (CCD, QEPro, Ocean Optics) for the spectral distribution; or a digital camera (Canon EOS 6D DSLR camera, fitted with a Tonika AT-X PRO MACRO 100 mm f/2.8 D lens) for images.

3D ECL data (intensity versus emission wavelength and applied potential) were obtained using an automated procedure created in Nova software (Figure S1, see Supporting Information). A series of 10 s pulses of increasing potential were interspersed with 10 s at 0 V. ECL spectra were acquired at each applied oxidative potential by synchronising the CCD detector with the electrochemical experiment via an HR4000 (Ocean Optics) break-out box. Presented data are the average of at least three replicate experiments, for which the relative standard deviation (based on the area of the spectrum collected at the potential that elicited the greatest ECL intensity) was generally less than 6%.

The ECL spectra were then deconvoluted (Figure S2), where the concentrations of each metal complex (c_{Ru} for the Ru(II) complex, and c_{Ir} for the Ir(III) complex) were determined by minimising the sum of the magnitude difference between the model ($I_{total} = c_{Ru}I_{Ru} + c_{Ir}I_{Ir}$) and measured intensity (I_{meas}) at each wavelength. Contour plots of the raw and deconvoluted data were created using OriginPro (OriginLab, USA). Profiles of ECL intensity versus applied potential were obtained from the raw and deconvoluted data by integrating the ECL spectral distribution at each applied potential (Figure S2).

3. Results and discussion

3.1. Characterisation of the iridium(III) complexes

Compared to $[Ir(sppy)_3]^{3-}$ and $[Ir(ppy)_2(pt\text{-}TEG)]^+$, the fluorinated derivatives are hypsochromically shifted (Table 1, Figures S3, S4). Their photoluminescence has less overlap with that of $[Ru(bpy)_3]^{2+}$, which would improve their resolution in multi-luminophore systems, but greater overlap with the visible absorption of $[Ru(bpy)_3]^{2+}$, where more efficient energy transfer may be anticipated. Conversely, the luminescence of the $[Ir(bt)_2(pt\text{-}TEG)]^+$ complex is at longer wavelengths than the other Ir(III) complexes, although still distinguishable from the emission of $[Ru(bpy)_3]^{2+}$, with almost no overlap with the absorption bands of $[Ru(bpy)_3]^{2+}$. Low temperature photoluminescence spectra (Figure S5) were used to estimate the energy between the zeroth vibrational levels of the ground and triplet excited state responsible for the emission ($E_{0\text{–}0}$; Table 1), which in conjunction with the ground state electrochemical potentials (vide infra), can be used to derive the potentials of the excited state ($M^{0*/-}$ and $M^{+/0*}$; Table S1) [38]. These not only provide insight into oxidative and reductive quenching of the excited state, but also the reverse process: the energy required to attain the excited state from the reduced or oxidised complex [26]. For example, for the reaction depicted in Scheme 4 (Fig. 1) to be energetically feasible, the potential for $M^{0*/-}$ must be lower in magnitude than that of the reduction of $TPrA^{\bullet+}$ (0.89 ± 0.06 V vs Ag/AgCl [5]). Low temperature spectra for $[Ir(f\text{-}sppy)_3]^{3-}$ and $[Ir(df\text{-}sppy)_3]^{3-}$ had not previously been reported, but the $E_{0\text{–}0}$ derived from this approach were

Table 1
Selected properties of $[Ru(bpy)_3]^{2+}$ and the iridium(III) complexes.

	Photoluminescence				Electrochemistry and ECL		
	λ_{max}/nm (r.t.)[a]	λ_{max}/nm (85 K)[b]	E_{0-0} /eV[c]	ϕ_{PL}[d]	E_{ox}/V (vs Ag/AgCl)	E_{red}/V (vs Ag/AgCl)	I_{ECL}
$[Ru(bpy)_3]^{2+}$	**625**	581	2.13	0.063	1.08[e,h]	−1.35[f,h]	1
$[Ir(bt)_2(pt\text{-}TEG)]^{+}$	526, **562**	515	2.41	0.23	1.28[e,i]	−1.67[f,h]	2.76[j]
$[Ir(df\text{-}ppy)_2(pt\text{-}TEG)]^{+}$	452, **481**	448	2.77	0.13	1.44[e,i]	−1.75[f,h]	0.26[j]
$[Ir(ppy)_2(pt\text{-}TEG)]^{+}$	475, **505**	471	2.63	0.14	1.08[e,i]	−1.82[f,h]	1.57[j], 0.37 [k]
$[Ir(sppy)_3]^{3-}$	**517**	481	2.58	0.73	0.79[e,h]	−2.05[g,i]	0.01[k]
$[Ir(f\text{-}sppy)_3]^{3-}$	**494**	460	2.70	0.91	0.93[e,h]	−2.17[g,h]	0.03[k]
$[Ir(df\text{-}sppy)_3]^{3-}$	**484**	449	2.76	0.84	1.08[e,h]	−2.08[g,i]	0.05[k]

[a]Most intense peak in bold. [b]Shortest wavelength peak only. [c]From λ_{max}/nm (85 K). [d]From references [29,33,39,40]. [e]In aqueous phosphate buffer (0.1 M; pH 7.5). [f]In acetonitrile with 0.1 M $TBAPF_6$. [g]In DMF with 0.1 M $TBAPF_6$. [h]Chemically reversible. [i]Chemically irreversible. [j]Relative to $[Ru(bpy)_3]^{2+}$ (10 μM metal complex in phosphate buffer (pH 7.5) with 10 mM TPrA; 10 s at 10 Hz, E_{pa} + 0.1 V; integrated ECL spectra collected using a CCD spectrometer [29]. [k]Relative to $[Ru(bpy)_3]^{2+}$ (10 μM metal complex in ProCell solution (180 mM TPrA, pH 6.8); 10 s single pulse at 1.2 V vs Ag/AgCl; integrated ECL spectra collected using a CCD spectrometer).

similar to the values of 2.76 eV and 2.81 eV estimated from the short-wavelength edges (at 10% intensity) of their emission spectra in water at ambient temperature [33].

In aqueous solution, the $[Ir(C^N)_2(pt\text{-}TEG)]^{+}$ complexes exhibit chemically irreversible oxidation at potentials greater or equal to the reversible oxidation of $[Ru(bpy)_3]^{2+}$ (Figs. 3, S6). Due to the limited electrochemical window of the aqueous phosphate buffer, the potentials at which these complexes are reduced was assessed in acetonitrile. Under these conditions, the reductions were chemically reversible at similar potentials to that estimated for the oxidation of TPrA$^{\bullet}$ (Figs. 3, S7). In contrast, $[Ir(sppy)_3]^{3-}$ and its fluorinated derivatives exhibited reversible oxidations in aqueous solution at potentials lesser or equal to $[Ru(bpy)_3]^{2+}$ (Figs. 3, S8). Their reductions (assessed in dimethylformamide due to their insolubility in acetonitrile) were largely irreversible and far beyond the potential at which TPrA$^{\bullet}$ is oxidised (Figs. 3, S9).

The ECL properties of $[Ir(sppy)_3]^{3-}$ and the $[Ir(C^N)_2(pt\text{-}TEG)]^{+}$ complexes with TPrA as a co-reactant have been previously investigated [9,28,29]. Some examples of intensities relative to that of $[Ru(bpy)_3]^{2+}$ under specific conditions are shown in Table 1. The ECL of $[Ir(f\text{-}sppy)_3]^{3-}$ and $[Ir(df\text{-}sppy)_3]^{3-}$, however, had not been explored. We examined the co-reactant ECL of these complexes in ProCell solution (containing 180 mM TPrA), in comparison to $[Ir(sppy)_3]^{3-}$ and $[Ru(bpy)_3]^{2+}$. The integrated ECL peak intensities for $[Ir(sppy)_3]^{3-}$, $[Ir(f\text{-}sppy)_3]^{3-}$, and $[Ir(df\text{-}sppy)_3]^{3-}$, measured with an extended range PMT, were 1.4%, 4.7%, and 7.7% that of $[Ru(bpy)_3]^{2+}$ (Figure S10; Table S2). The ECL intensities (integrated spectra) acquired with a CCD spectrometer were lower (0.9%, 2.8% and 4.8%, respectively, relative to $[Ru(bpy)_3]^{2+}$; Figure S11), which can be attributed to the more uniform sensitivity of this photodetector over the wavelength range. Photographs of the ECL emissions at the working electrode surface are also shown in Table S2.

3.2. *Electrochemiluminescence enhancers: $[Ir(sppy)_3]^{3-}$ and its fluorinated derivatives*

In our previous exploration of $[Ir(sppy)_3]^{3-}$ as an enhancer of the ECL of $[Ru(bpy)_3]^{2+}$ with TPrA co-reactant [9], we applied an electrochemical potential pulse sequence for the collection of ECL spectra over a series of increasing potentials, which were presented as contour plots. Spectra at two potentials, 0.9 V and 1.2 V vs Ag/AgCl, were then deconvoluted into the characteristic emissions of the two complexes to quantitatively assess the influence of $[Ir(sppy)_3]^{3-}$ on the ECL intensity of $[Ru(bpy)_3]^{2+}$.

For a more comprehensive evaluation in the current study, we have used a similar pulse sequence between 0.7 V and 1.6 V vs Ag/AgCl (Figure S1), and developed a simple procedure to deconvolute the spectra at all applied potentials (Figure S2). The integrated ECL intensity of the deconvoluted spectra can then be compared to that of $[Ru(bpy)_3]^{2+}$ in the absence of the Ir(III) complex. The ECL intensities of $[Ru(bpy)_3]^{2+}$ in ProCell solution, with and without $[Ir(sppy)_3]^{3-}$, over the applied potential range are shown in Fig. 4a. Similar to our previous report, the ECL intensity of $[Ru(bpy)_3]^{2+}$ was enhanced by 9-fold at 0.9 V, and 2-fold at 1.2 V by the addition of $[Ir(sppy)_3]^{3-}$. The redox mediator has a greater effect at 0.9 V for two reasons: Firstly, at low potentials, ECL arises from the 'indirect pathway' (Scheme 3, Fig. 1), in which the mediator can act as an alternative oxidant to generate the

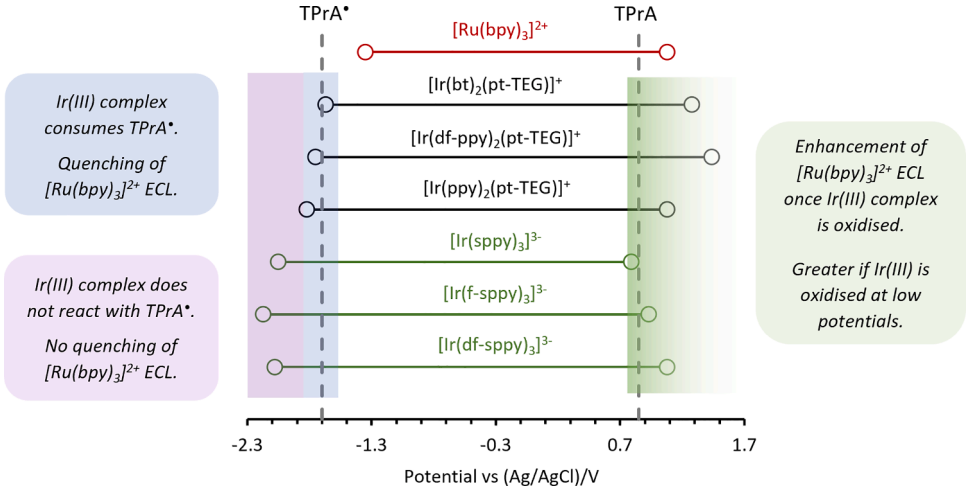

Fig. 3. Potentials at which the metal complexes are oxidised (right) and reduced (left) in comparison to those of the oxidation of TPrA and the α-amino alkyl radical TPrA$^{\bullet}$ (dotted lines). Metal complex oxidation potentials were determined in aqueous solution, whereas the reduction potentials were measured in acetonitrile ($[Ru(bpy)_3]^{2+}$ and $[Ir(C^N)_2(pt\text{-}TEG)]^{+}$ complexes) or dimethylformamide ($[Ir(sppy)_3]^{3-}$ and its derivatives).

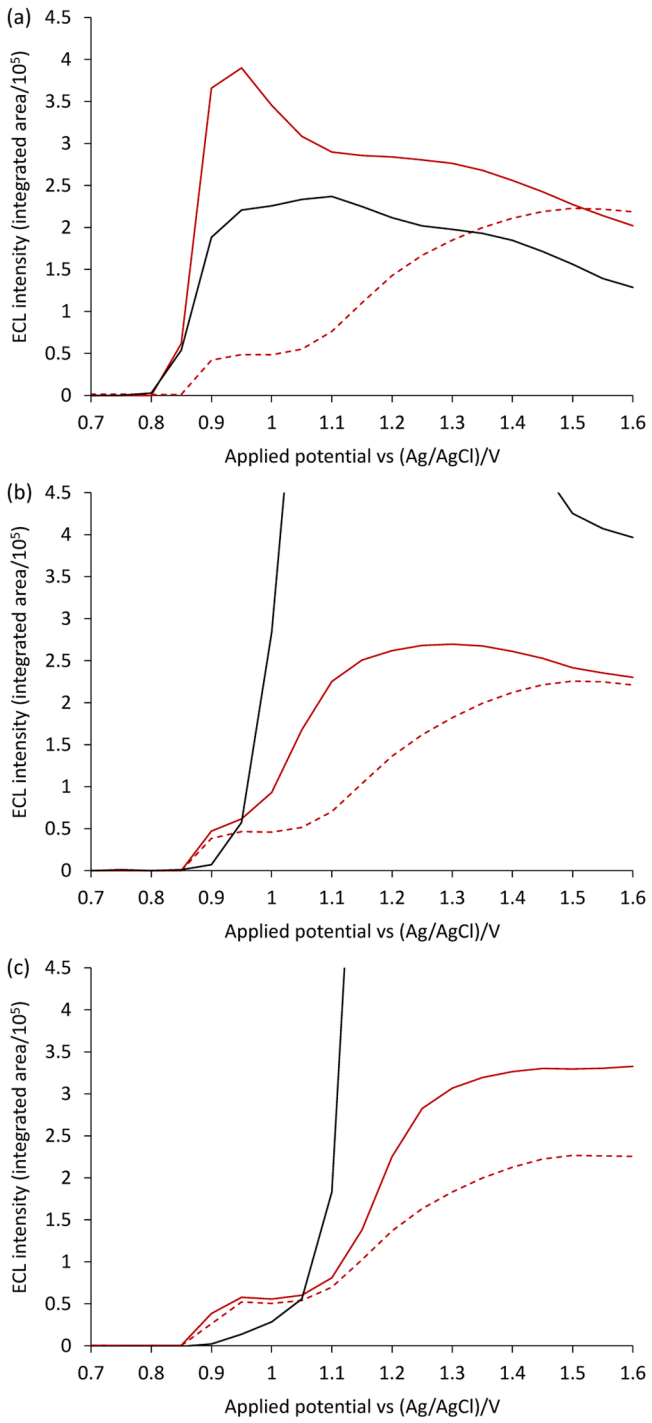

Fig. 4. ECL intensities (integrated spectra) of 1 μM $[Ru(bpy)_3]^{2+}$ (solid red plots) and 100 μM (a) $[Ir(sppy)_3]^{3-}$, (b) $[Ir(f\text{-}sppy)_3]^{3-}$, or (c) $[Ir(df\text{-}sppy)_3]^{3-}$ (black plots) from a mixture of the complexes in ProCell solution, after deconvolution of their emissions at each applied potential. The dashed red plots show the corresponding ECL intensity of 1 μM $[Ru(bpy)_3]^{2+}$ in ProCell without the Ir(III) complex. The full plots for the Ir(III) complexes are shown in Figure S13.

excited state (Scheme 5), whereas at higher potentials, the 'direct' pathway (Scheme 1) is dominant. Secondly, the mediator serves as an electrocatalyst for co-reactant oxidation, which is less competitive with heterogeneous oxidation when the overpotential is greater [10,32].

Greater enhancement can be obtained at higher concentrations of $[Ir(sppy)_3]^{3-}$, but 100 μM was deemed most appropriate considering the amount consumed in experiments, the diminishing improvement in signal as the Ir(III) complex concentration is increased [32], and the intensity of the ECL arising from $[Ir(sppy)_3]^{3-}$ (via Scheme 1, where M = $[Ir(sppy)_3]^{3-}$), which was exploited as an internal standard in our previous study [9]. We therefore initially examined all Ir(III) complexes in the current study at a concentration of 100 μM.

The $[Ir(f\text{-}sppy)_3]^{3-}$ and $[Ir(df\text{-}sppy)_3]^{3-}$ complexes also enhanced the ECL of $[Ru(bpy)_3]^{2+}$ (red plots in Fig. 4), but only once the potentials required for their oxidation were applied (Fig. 3; Table 1), and to a lesser extent: 3.3-fold at 1.05 V by $[Ir(f\text{-}sppy)_3]^{3-}$ and 1.7-fold at 1.25 V by $[Ir(df\text{-}sppy)_3]^{3-}$. However, the $[Ir(df\text{-}sppy)_3]^{3-}$ complex was the only Ir(III) species that significantly increased the ECL of $[Ru(bpy)_3]^{2+}$ at the highest applied potential (1.6 V vs Ag/AgCl), which may be useful for some multi-colour ECL applications. The corresponding ECL contour plots showing the full data sets without deconvolution are in Figure S12.

As with $[Ir(sppy)_3]^{3-}$, the enhancement by $[Ir(f\text{-}sppy)_3]^{3-}$ and $[Ir(df\text{-}sppy)_3]^{3-}$ coincided with the onset of ECL from the Ir(III) complex in the mixture (black plots in Figs. 4 and S13) via the pathway depicted in Scheme 1 (where M = $[Ir(sppy)_3]^{3-}$ or its fluorinated derivative). These three Ir(III) complexes (unlike $[Ru(bpy)_3]^{2+}$) cannot proceed via Schemes 3 or 4 because they are not reduced by $TPrA^{\bullet}$ (i.e. their E_{red} fall into the zone indicated in purple in Fig. 3).

3.3. $[Ir(C\hat{}N)_2(pt\text{-}TEG)]^+$ complexes as enhancers or quenchers

The three $[Ir(C\hat{}N)_2(pt\text{-}TEG)]^+$ complexes also increased the ECL of $[Ru(bpy)_3]^{2+}$ once the potentials required to oxidise the Ir(III) complex were applied (Figs. 5 and S14). As observed with the Ir(III) complexes containing sulfonated phenylpyridines, the higher the E_{ox} of the Ir(III) complex, the lesser the degree of enhancement (1.4-, 1.2- and 1.1-fold by $[Ir(ppy)_2(pt\text{-}TEG)]^+$, $[Ir(bt)_2(pt\text{-}TEG)]^+$ and $[Ir(df\text{-}ppy)_2(pt\text{-}TEG)]^+$ at applied potentials of 1.25 V, 1.45 V and 1.50 V, respectively, which were far lower than the 9-fold enhancement by $[Ir(f\text{-}sppy)_3]^{3-}$ at 0.90 V).

In our previous ECL microscopy study of $[Ru(bpy)_3]^{2+}$ immobilised on magnetic beads [32], the addition of 100 μM $[Ir(bt)_2(pt\text{-}TEG)]^+$ or $[Ir(df\text{-}ppy)_2(pt\text{-}TEG)]^+$ to the solution diminished the ECL of the Ru(II) complex by 65% and 24%, respectively, when applying potentials sufficient to oxidise the Ir(III) complexes (1.3 V and 1.5 V vs Ag/AgCl). Even greater quenching (71% and 75%) was observed when applying a potential (1.2 V) below their E_{ox}. The attenuation of the $[Ru(bpy)_3]^{2+}$ ECL was ascribed to the reduction of the Ir(III) complexes by $TPrA^{\bullet}$ (Fig. 2) [32], thereby consuming this essential intermediate of the pathway (Scheme 4) required for ECL from immobilised luminophores [5], irrespective of the applied potential.

In the current study, all reactants can diffuse freely in solution, and $[Ru(bpy)_3]^{2+}$ is electrochemically oxidised at potentials above its E_{ox} (1.08 V vs Ag/AgCl), enabling Schemes 1-3 (where M = $[Ru(bpy)_3]^{2+}$). Moreover, as $[Ru(bpy)_3]^{2+}$ is in the immediate vicinity of the electrogenerated TPrA radicals as they are formed, their reactions (including within Scheme 5, at potentials sufficient to oxidise $[Ir(C\hat{}N)_2(pt\text{-}TEG)]^+$) are more competitive. Consequently, in contrast to the prior observations with the bead-based format, the ECL of $[Ru(bpy)_3]^{2+}$ was enhanced at high potentials by the addition of the $[Ir(C\hat{}N)_2(pt\text{-}TEG)]^+$ complexes (Fig. 5). At potentials below the E_{ox} of $[Ru(bpy)_3]^{2+}$, ECL is restricted to Scheme 4 (M = $[Ru(bpy)_3]^{2+}$) [5] and the electrochemical oxidation of TPrA occurs at a slower rate. Under these conditions, the reaction of $TPrA^{\bullet}$ with $[Ir(C\hat{}N)_2(pt\text{-}TEG)]^+$ is dominant due to the higher concentration of the Ir(III) complex, resulting in quenching of the ECL of $[Ru(bpy)_3]^{2+}$ (Fig. 5).

The ECL of the $[Ir(C\hat{}N)_2(pt\text{-}TEG)]^+$ complexes in the reaction mixtures (black plots in Figs. 5 and S15) were much more intense than that of $[Ir(sppy)_3]^{3-}$ and its derivatives. We also examined the ECL of 1 μM $[Ru(bpy)_3]^{2+}$ and 10 μM $[Ir(C\hat{}N)_2(pt\text{-}TEG)]^+$ in ProCell solution (Figures S16 and S17). Under those conditions, the ECL intensities of the two luminophores were similar, but the influence of the Ir(III)

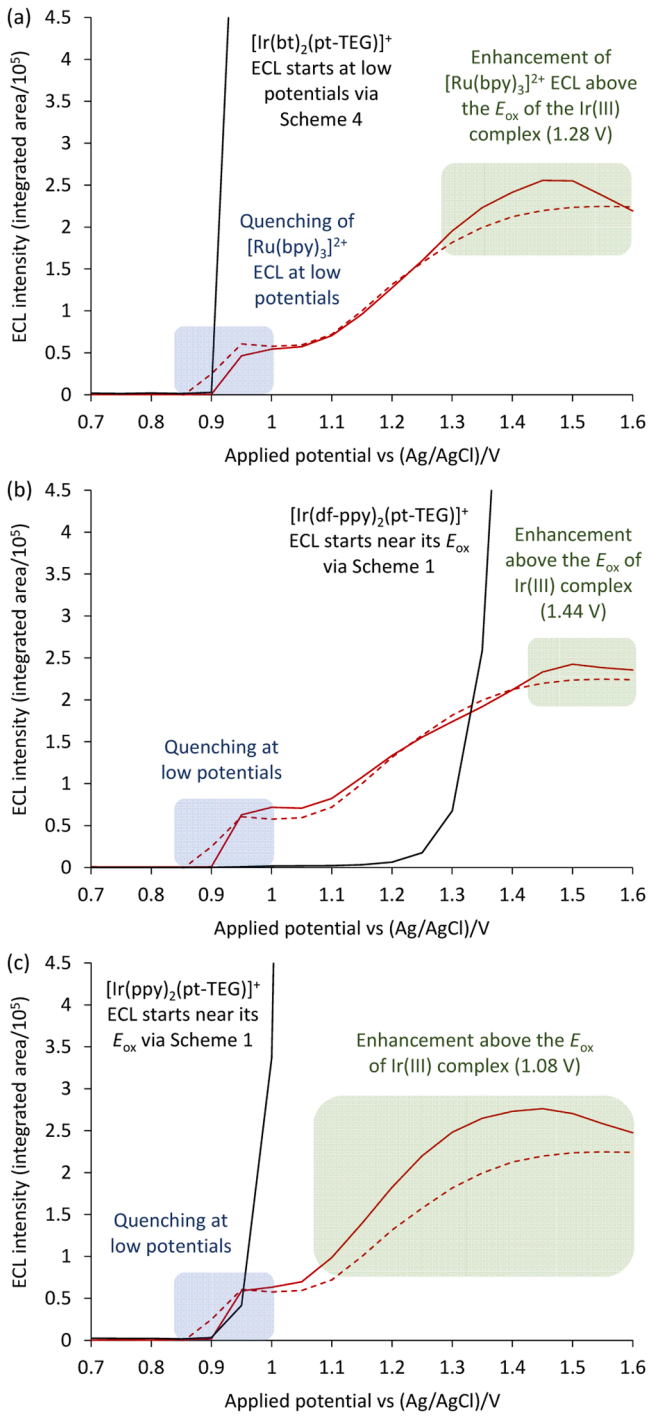

Fig. 5. ECL intensities (integrated spectral distribution) of 1 μM $[Ru(bpy)_3]^{2+}$ (solid red plots) and 100 μM (a) $[Ir(bt)_2(pt\text{-}TEG)]^+$, (b) $[Ir(df\text{-}ppy)_2(pt\text{-}TEG)]^+$, or (c) $[Ir(ppy)_2(pt\text{-}TEG)]^+$ (black plots) from a mixture of the complexes in ProCell solution, after deconvolution of their emissions at each applied potential. The dashed red plots show the corresponding ECL intensity of 1 μM $[Ru(bpy)_3]^{2+}$ in ProCell without the Ir(III) complex. The full plots for the Ir(III) complexes are shown in Figure S15.

complexes on the ECL of $[Ru(bpy)_3]^{2+}$ was greatly diminished.

The ECL of $[Ir(bt)_2(pt\text{-}TEG)]^+$ appears as two 'waves' as the applied potential is increased (Figure S15a): the first emerges at the E_{ox} of TPrA (0.89 V vs Ag/AgCl [5]) and the second at the E_{ox} of the Ir(III) complex (1.28 V vs Ag/AgCl). Based on the data in Table 1, Schemes 1–4 (where M = $[Ir(bt)_2(pt\text{-}TEG)]^+$) are all feasible. The first and second waves of ECL therefore arise from Schemes 4 and 1–3, respectively. The efficient first wave ECL from this complex confirms the consumption of $TPrA^\bullet$ as the mechanism of quenching of the ECL from $[Ru(bpy)_3]^{2+}$.

The $[Ir(df\text{-}ppy)_2(pt\text{-}TEG)]^+$ complex is also reduced by $TPrA^\bullet$ (as predicted in Fig. 3, and confirmed by its quenching of the ECL of $[Ru(bpy)_3]^{2+}$), but the subsequent reaction of $[Ir(df\text{-}ppy)_2(pt\text{-}TEG)]^0$ (M^-) and $TPrA^{\bullet+}$ in Scheme 4 is not sufficiently energetic to attain the excited state $[Ir(df\text{-}ppy)_2(pt\text{-}TEG)]^{+}*$ (i.e. $E([Ir(df\text{-}ppy)_2(pt\text{-}TEG)]^{0/+*}) < E(TPrA^{+/0})$; See Table S2). Therefore, the ECL of $[Ir(df\text{-}ppy)_2(pt\text{-}TEG)]^+$ is only seen via Schemes 1–3 at applied potentials sufficient to oxidise the Ir(III) complex.

$[Ir(ppy)_2(pt\text{-}TEG)]^+$ was selected for the study as an $[Ir(C\hat{}N)_2(pt\text{-}TEG)]^+$ complex with an E_{red} beyond the potential at which the $TPrA^\bullet$ is oxidised. However, the difference in these potentials is within the error associated with their estimation, and the quenching of the ECL of $[Ru(bpy)_3]^{2+}$ by this complex at low potentials (Fig. 5c) shows that it reacts with $TPrA^\bullet$ efficiently. The subsequent reaction of $[Ir(ppy)_2(pt\text{-}TEG)]^0$ (M^-) and $TPrA^{\bullet+}$ in Scheme 4 to attain the excited state $[Ir(ppy)_2(pt\text{-}TEG)]^{+}*$ is also a borderline case (i.e. $E([Ir(ppy)_2(pt\text{-}TEG)]^{0/+*}) \approx E(TPrA^{+/0})$; See Table S2). The absence of 'first wave' ECL for $[Ir(ppy)_2(pt\text{-}TEG)]^+$ (compare Figure S15c to Figure S15a) reveals that the ECL mechanisms of this complex are limited to Schemes 1–3 (where M = $[Ir(ppy)_2(pt\text{-}TEG)]^+$).

This complex was also selected because its E_{ox} is lower than those of $[Ir(bt)_2(pt\text{-}TEG)]^+$ and $[Ir(df\text{-}ppy)_2(pt\text{-}TEG)]^+$, which we anticipated would improve the enhancement of the ECL of $[Ru(bpy)_3]^{2+}$. This was indeed the case, but the improvement was less than that of $[Ir(df\text{-}sppy)_3]^{3-}$, for which the same E_{ox} was estimated. This can be rationalised by: (i) the irreversibility of the oxidation of $[Ir(ppy)_2(pt\text{-}TEG)]^+$ (Figure S6c vs S8c); (ii) the more efficient reaction of $[Ir(ppy)_2(pt\text{-}TEG)]^{2+}$ than $[Ir(df\text{-}sppy)_3]^{2-}$ with $TPrA^\bullet$ to generate their respective emitting species in Scheme 1 (where M = the Ir(III) complex), as seen in their relative ECL intensities (Figure S15c vs S13c), which compete with their reactions with $[Ru(bpy)_3]^+$ to generate $[Ru(bpy)_3]^{2+}*$ (Scheme 5, where M = $[Ru(bpy)_3]^{2+}$ and E = $[Ir(df\text{-}sppy)_3]^{3-}$); and/or (iii) the negative charge on the oxidised $[Ir(df\text{-}sppy)_3]^{2-}$ complex, promoting its reaction with $[Ru(bpy)_3]^+$ in Scheme 5.

4. Conclusions

We investigated the ECL enhancement or quenching of the widely applied $[Ru(bpy)_3]^{2+}$ and TPrA system in the presence of different Ir(III) complexes and rationalised the behaviour by considering the applied potentials, the electrochemical and photochemical properties of the complexes, and the energy requirements of the reaction pathways. The greatest enhancement of the co-reactant ECL of $[Ru(bpy)_3]^{2+}$ was obtained from Ir(III) complexes exhibiting: (i) an E_{ox} nearest the potential at which TPrA is oxidised (the green-coloured zone in Fig. 3), and (ii) an E_{red} well beyond the estimated reduction strength of $TPrA^\bullet$ (the purple-coloured zone in Fig. 3). The addition of fluorine substituents on the phenylpyridine ligands of the Ir(III) complexes increases their E_{ox}, which diminishes their enhancement of the ECL of $[Ru(bpy)_3]^{2+}$, despite the greater overlap of their emission with the visible absorption bands of $[Ru(bpy)_3]^{2+}$. Energy transfer, therefore, does not make a significant contribution relative to the electron-transfer ('redox mediator') pathways (Scheme 5: M = $[Ru(bpy)_3]^{2+}$ and E = Ir(III) complex; and Scheme 2: M = Ir(III) complex). Concomitant ECL from the Ir(III) complexes that meet the above criteria can only occur through a pathway involving their oxidation (Scheme 1: M = Ir(III) complex), which competes with their enhancement of $[Ru(bpy)_3]^{2+}$ ECL.

Iridium(III) complexes that are reduced by $TPrA^\bullet$ (such as those with an E_{red} in the blue-coloured zone in Fig. 3) quench the co-reactant ECL of $[Ru(bpy)_3]^{2+}$ under conditions where its initial reduction is essential (i.e. Scheme 4: M = $[Ru(bpy)_3]^{2+}$). These include: (i) the application of potentials sufficient to oxidise TPrA but not $[Ru(bpy)_3]^{2+}$; and (ii) in the bead-based assay format irrespective of the applied potential. If the reduced Ir(III) complex reacts with $TPrA^{\bullet+}$ with sufficient energy to generate the excited state Ir(III) complex, its ECL can be observed upon

oxidation of TPrA (such as for $[Ir(bt)_2(pt\text{-}TEG)]^+$); if not, its ECL can only be attained at the potentials sufficient for its oxidation (such as for $[Ir(df\text{-}ppy)_2(pt\text{-}TEG)]^+$). These energy requirements can be assessed through the ground and excited state redox potentials.

This study provides a new understanding of the influence of Ir(III) complexes on the coreactant ECL of $[Ru(bpy)_3]^{2+}$ in ProCell solution, which will inform the future design and application of redox mediators in this widely used ECL system.

CRediT authorship contribution statement

Steven J. Blom: Writing – review & editing, Writing – original draft, Investigation, Formal analysis, Data curation. **Natasha S. Adamson:** Writing – review & editing, Writing – original draft, Investigation, Formal analysis, Data curation. **Emily Kerr:** Writing – review & editing, Supervision, Funding acquisition, Conceptualization. **Egan H. Doeven:** Writing – review & editing, Supervision, Methodology, Conceptualization. **Oliver S. Wenger:** Writing – review & editing, Supervision, Resources, Project administration. **Raoul S. Schaer:** Writing – review & editing, Investigation, Data curation. **David J. Hayne:** Writing – review & editing, Investigation, Data curation. **Francesco Paolucci:** Writing – review & editing, Formal analysis, Conceptualization. **Neso Sojic:** Writing – review & editing, Formal analysis, Conceptualization. **Giovanni Valenti:** Writing – review & editing, Formal analysis, Conceptualization. **Paul S. Francis:** Writing – review & editing, Writing – original draft, Supervision, Resources, Project administration, Funding acquisition, Formal analysis, Conceptualization.

Declaration of competing interest

The authors declare that they have no known competing financial interests or personal relationships that could have appeared to influence the work reported in this paper.

Data availability

Data will be made available on request.

Acknowledgements

The authors thank the Australian Research Council (DP200102947; DP220100300) for funding this work. E. K. gratefully acknowledges the National Health and Medical Research Council of Australia (GNT1161573).

Supplementary materials

Supplementary material associated with this article can be found, in the online version, at doi:10.1016/j.electacta.2024.143957.

References

[1] Analytical electrogenerated chemiluminescence: from fundamentals to bioassays, in: N. Sojic (Ed.), Royal Society of Chemistry, Cambridge, 2020, p. 501.
[2] J.B. Noffsinger, N.D. Danielson, Generation of chemiluminescence upon reaction of aliphatic amines with tris(2,2′-bipyridine)ruthenium(III), Anal. Chem. 59 (1987) 865–868.
[3] J.K. Leland, M.J. Powell, Electrogenerated chemiluminescence: an oxidative-reduction type ECL reaction sequence using tripropyl amine, J. Electrochem. Soc. 137 (1990) 3127–3131.
[4] F. Kanoufi, Y. Zu, A.J. Bard, Homogeneous oxidation of trialkylamines by metal complexes and its impact on electrogenerated chemiluminescence in the trialkylamine/$Ru(bpy)_3^{2+}$ system, J. Phys. Chem. B 105 (2001) 210–216.
[5] W. Miao, J.-P. Choi, A.J. Bard, Electrogenerated chemiluminescence 69: the tris (2,2′-bipyridine)ruthenium(II), ($Ru(bpy)_3^{2+}$)/tri-*n*-propylamine (TPrA) system revisited - a new route involving $TPrA^{\bullet+}$ cation radicals, J. Am. Chem. Soc. 124 (2002) 14478–14485.
[6] E. Kerr, E.H. Doeven, P.S. Francis, Recent advances in mechanistic understanding and analytical methodologies of the electrochemiluminescence of tris(2,2′-bipyridine)ruthenium(II) and tri-*n*-propylamine, Curr. Opin. Electrochem. 35 (2022) 101034.
[7] E. Villani, K. Sakanoue, Y. Einaga, S. Inagi, A. Fiorani, Photophysics and electrochemistry of ruthenium complexes for electrogenerated chemiluminescence, J. Electroanal. Chem. 921 (2022) 116677.
[8] Y. Zu, A.J. Bard, Electrogenerated chemiluminescence. 66. The role of direct coreactant oxidation in the ruthenium tris(2,2′)bipyridyl/tripropylamine system and the effect of halide ions on the emission intensity, Anal. Chem. 72 (2000) 3223–3232.
[9] E. Kerr, D.J. Hayne, L.C. Soulsby, J.C. Bawden, S.J. Blom, E.H. Doeven, L. C. Henderson, C.F. Hogan, P.S. Francis, A redox-mediator pathway for enhanced multicolour electrochemiluminescence in aqueous solution, Chem. Sci. 13 (2022) 469–477.
[10] E. Kerr, S. Knezevic, P.S. Francis, C.F. Hogan, G. Valenti, F. Paolucci, F. Kanoufi, N. Sojic, Electrochemiluminescence amplification in bead-based assays induced by a freely diffusing iridium(III) complex, ACS Sens. 8 (2023) 933–939.
[11] E. Faatz, A. Finke, H.-P. Josel, G. Prencipe, S. Quint, M. Windfuhr, Automated immunoassays for the detection of biomarkers in body fluids, in: N. Sojic (Ed.), Analytical Electrogenerated Chemiluminescence: From Fundamentals to Bioassays, The Royal Society of Chemistry, 2020, pp. 443–470.
[12] A. Zanut, A. Fiorani, S. Canola, T. Saito, N. Ziebart, S. Rapino, S. Rebeccani, A. Barbon, T. Irie, H.-P. Josel, F. Negri, M. Marcaccio, M. Windfuhr, K. Imai, G. Valenti, F. Paolucci, Insights into the mechanism of coreactant electrochemiluminescence facilitating enhanced bioanalytical performance, Nat. Commun. 11 (2020) 2668.
[13] M. Sentic, M. Milutinovic, F. Kanoufi, D. Manojlovic, S. Arbault, N. Sojic, Mapping electrogenerated chemiluminescence reactivity in space: mechanistic insight into model systems used in immunoassays, Chem. Sci. 5 (2014) 2568–2572.
[14] X. Liu, L. Shi, W. Niu, H. Li, G. Xu, Environmentally friendly and highly sensitive ruthenium(II) tris(2,2′-bipyridyl) electrochemiluminescent system using 2-(dibutylamino)ethanol as co-reactant, Angew. Chem., Int. Ed. 46 (2007) 421–424.
[15] G.J. Barbante, N. Kebede, C.M. Hindson, E.H. Doeven, E.M. Zammit, G.R. Hanson, C.F. Hogan, P.S. Francis, Control of excitation and quenching in multi-colour electrogenerated chemiluminescence systems through choice of co-reactant, Chem. Eur. J. 20 (2014) 14026–14031.
[16] N. Kebede, P.S. Francis, G.J. Barbante, C.F. Hogan, Electrogenerated chemiluminescence of tris(2,2′-bipyridine)ruthenium(II) using common biological buffers as co-reactant, pH buffer and supporting electrolyte, Analyst 140 (2015) 7142–7145.
[17] S.A. Kitte, C. Wang, S. Li, Y. Zholudov, L. Qi, J. Li, G. Xu, Electrogenerated chemiluminescence of tris(2,2′-bipyridine)ruthenium(II) using *N*-(3-aminopropyl) diethanolamine as coreactant, Anal. Bioanal. Chem. 408 (2016) 7059–7065.
[18] S. Kirschbaum-Harriman, M. Mayer, A. Duerkop, T. Hirsch, A.J. Baeumner, Signal enhancement and low oxidation potentials for miniaturized ECL biosensors via N-butyldiethanolamine, Analyst 142 (2017) 2469–2474.
[19] M. Staffilani, E. Höss, U. Giesen, E. Schneider, F. Hartl, H.-P. Josel, L. De Cola, Multimetallic ruthenium(II) complexes as electrochemiluminescent labels, Inorg. Chem. 42 (2003) 7789–7798.
[20] D.N. Lee, H.S. Park, E.H. Kim, Y.M. Jun, J.-Y. Lee, W.-Y. Lee, B.H. Kim, Synthesis of novel electrochemiluminescent polyamine dendrimers functionalized with polypyridyl Ru(II) complexes and their electrochemical properties, Bull. Korean Chem. Soc. 27 (2006) 99–105.
[21] Y. Feng, F. Sun, N. Wang, J. Lei, H. Ju, $Ru(bpy)_3^{2+}$ incorporated luminescent polymer dots: double-enhanced electrochemiluminescence for detection of single-nucleotide polymorphism, Anal. Chem. 89 (2017) 7659–7666.
[22] A. Zanut, F. Palomba, M.R. Scota, S. Rebeccani, M. Marcaccio, D. Genovese, E. Rampazzo, G. Valenti, F. Paolucci, L. Prodi, Dye-doped silica nanoparticles for enhanced ECL-based immunoassay analytical performance, Angew. Chem. Int. Ed. 59 (2020) 21858–21863.
[23] A. Kapturkiewicz, Cyclometalated iridium(III) chelates—a new exceptional class of the electrochemiluminescent luminophores, Anal. Bioanal. Chem. 408 (2016) 7013–7033.
[24] S. Laird, C.F. Hogan, Electrochemiluminescence of iridium complexes, in: E. Zysman-Colman (Ed.), Iridium(III) in Optoelectronic and Photonics Applications, John Wiley & Sons, Inc., Chichester, UK, 2017, pp. 359–414.
[25] S. Voci, R. Duwald, S. Grass, D.J. Hayne, L. Bouffier, P.S. Francis, J. Lacour, N. Sojic, Self-enhanced multicolor electrochemiluminescence by competitive electron-transfer processes, Chem. Sci. 11 (2020) 4508–4515.
[26] E. Kerr, E.H. Doeven, D.J.D. Wilson, C.F. Hogan, P.S. Francis, Considering the chemical energy requirements of the tri-*n*-propylamine co-reactant pathways for the judicious design of new electrogenerated chemiluminescence detection systems, Analyst 141 (2016) 62–69.
[27] L. Yu, Z. Huang, Y. Liu, M. Zhou, Photophysics, electrochemistry and electrochemiluminescence of water-soluble biscyclometalated iridium (III) complexes, J. Organomet. Chem. 718 (2012) 14–21.
[28] E. Kerr, E.H. Doeven, G.J. Barbante, T.U. Connell, P.S. Donnelly, D.J.D. Wilson, T. D. Ashton, F.M. Pfeffer, P.S. Francis, Blue electrogenerated chemiluminescence from water-soluble iridium complexes containing sulfonated phenylpyridine or tetraethylene glycol derivatised triazolylpyridine ligands, Chem. Eur. J. 21 (2015) 14987–14995.
[29] L. Chen, D.J. Hayne, E.H. Doeven, J. Agugiaro, D.J.D. Wilson, L.C. Henderson, T. U. Connell, Y.H. Nai, R. Alexander, S. Carrara, C.F. Hogan, P.S. Donnelly, P. S. Francis, A conceptual framework for the development of iridium(III) complex-based electrogenerated chemiluminescence labels, Chem. Sci. 10 (2019) 8654–8667.

[30] B. Newman, L. Chen, L.C. Henderson, E.H. Doeven, P.S. Francis, D.J. Hayne, Water-soluble iridium(III) complexes containing tetraethylene-glycol-derivatized bipyridine ligands for electrogenerated chemiluminescence detection, Front. Chem. 8 (2020) 583631.
[31] S. Knežević, E. Kerr, B. Goudeau, G. Valenti, F. Paolucci, P.S. Francis, F. Kanoufi, N. Sojic, Bimodal electrochemiluminescence microscopy of single cells, Anal. Chem. 95 (2023) 7372–7378.
[32] A. Fracassa, C.I. Santo, E. Kerr, S. Knezevic, D.J. Hayne, P.S. Francis, F. Kanoufi, N. Sojic, F. Paolucci, G. Valenti, Redox-mediated electrochemiluminescence enhancement for bead-based immunoassay, Chem. Sci. 15 (2024) 1150–1158.
[33] B. Pfund, D.M. Steffen, M.R. Schreier, M.-S. Bertrams, C. Ye, K. Börjesson, O. S. Wenger, C. Kerzig, UV light generation and challenging photoreactions enabled by upconversion in water, J. Am. Chem. Soc. 142 (2020) 10468–10476.
[34] L.C. Soulsby, D.J. Hayne, E.H. Doeven, D.J.D. Wilson, J. Agugiaro, T.U. Connell, L. Chen, C.F. Hogan, E. Kerr, J.L. Adcock, P.S. Donnelly, J.M. White, P.S. Francis, Mixed annihilation electrogenerated chemiluminescence of iridium(III) complexes, Phys. Chem. Chem. Phys. 20 (2018) 18995–19006.
[35] C. Mallet, A. Bolduc, S. Bishop, Y. Gautier, W.G. Skene, Unusually high fluorescence quantum yield of a homopolyfluorenylazomethine – towards a universal fluorophore, Phys. Chem. Chem. Phys. 16 (2014) 24382–24390.
[36] E. Kerr, E.H. Doeven, G.J. Barbante, C.F. Hogan, D.J. Hayne, P.S. Donnelly, P. S. Francis, New perspectives on the annihilation electrogenerated chemiluminescence of mixed metal complexes in solution, Chem. Sci. 7 (2016) 5271–5279.
[37] J.M. Fernandez-Hernandez, E. Longhi, R. Cysewski, F. Polo, H.-P. Josel, L. De Cola, Photophysics and electrochemiluminescence of bright cyclometalated Ir(III) complexes in aqueous solutions, Anal. Chem. 88 (2016) 4174–4178.
[38] W.E. Jones Jr., M.A. Fox, Determination of excited-state redox potentials by phase-modulated voltammetry, J. Phys. Chem. 98 (1994) 5095–5099.
[39] K. Suzuki, A. Kobayashi, S. Kaneko, K. Takehira, T. Yoshihara, H. Ishida, Y. Shiina, S. Oishi, S. Tobita, Reevaluation of absolute luminescence quantum yields of standard solutions using a spectrometer with an integrating sphere and a back-thinned CCD detector, Phys. Chem. Chem. Phys. 11 (2009) 9850–9860.
[40] M.R. Schreier, X. Guo, B. Pfund, Y. Okamoto, T.R. Ward, C. Kerzig, O.S. Wenger, Water-soluble tris(cyclometalated) iridium(III) complexes for aqueous electron and energy transfer photochemistry, Acc. Chem. Res. 55 (2022) 1290–1300.